

# Preparation of Mesoporous Carbon with different Pore Wall structure via a temperature-programmed route for Lithium Sulfur Battery

Jing Wang, Yechun Lan, Lei Yan, Yufan Li, Zhiqiang Shi\*

Tianjin Key Laboratory of Advanced Fibers and Energy Storage, College of Materials Science and Engineering, Tianjin Polytechnic University, 399 Binshui West Road, Tianjin 300387, P. R. China

\*E-mail: [shizhiqiang@tjpu.edu.cn](mailto:shizhiqiang@tjpu.edu.cn) (Z. Shi).

*Received:* 7 April 2018 / *Accepted:* 4 June 2018 / *Published:* 5 July 2018

---

Due to the high specific surface area and large pore volume, mesoporous carbon materials are appealing for research interests to promote the performance of Lithium sulfur battery (Li/S). Herein, a mesoporous carbon (MC-1000) material, with high specific surface area ( $1432 \text{ m}^2 \text{ g}^{-1}$ ) and large pore volume ( $2.894 \text{ cm}^3 \text{ g}^{-1}$ ), is prepared via situ template method (using MgO as template), followed by pyrolysis at  $1000 \text{ }^\circ\text{C}$  in nitrogen atmosphere. Temperature-programmed route is used to regulate the pore wall of MC-1000, and the modified MC-1000, MC-1300 and MC-1600 with similar specific surface area and pore volume are chosen for investigating the effect of micro-structure of MC on the performance of Li/S battery. HR-TEM images show graphited structure gradually formed with the regulated progress, and the increasing of pyrolyzation temperature may also improve the conductivity of MC and MC/S composites. With an appropriate sulfur loading, MC-1300 and MC-1600 both present superior discharge capacity. Notably, MC-1300 and MC-1600 display high capacity of  $1524 \text{ mAh g}^{-1}$  and  $1415 \text{ mAh g}^{-1}$ , respectively, which is close to the theoretical specific capacity of sulfur.

---

**Keywords:** mesoporous carbon, pore wall, shuttle effect, lithium sulfur, large pore volume

## 1. INTRODUCTION

Environmentally friendly power sources become an imperative requirement because of the global energy shortage and environmental pollution. Lithium–sulfur (Li–S) batteries have attracted more and more attentions in the last few years because their theoretical specific energy is as high as  $2600 \text{ Wh kg}^{-1}$ , meaning that the theoretical specific energy is 3~5 times than that of Li-ion batteries [1-4]. In addition, sulfur is abundant on the earth and low cost which facilitates their commercialization. However, in the cathode, significant limitation leads to low cycle performance and even raises serious

safety issues. Main problems focus on the low electric conductivity of sulfur and the large volume expansion of discharge products from S to  $\text{Li}_2\text{S}_2/\text{Li}_2\text{S}$ . Especially, the “shuttle effect” attributed to polysulfide dissolution in the electrolyte could cause gradual loss of active sulfur [5-7]. To overcome these issues, a variety of efforts have been attempted, for instance, constructing the nanostructure of sulfur-carbon composite, using innovation electrolyte with additives such as  $\text{LiNO}_3$  and modifying the surface of separator by coating.

Traditionally, micro/mesoporous carbon [8,9], carbon nanotubes [10-13], graphene or its composites [14,15] are usually used as the cathode materials followed by sulfur loading. Porous carbon (PC), with high surface area and large pore volume has shown superiority of transporting ion. Moreover, its open-framework structure not only provides the reaction space but also avoids the adverse effects of electrolyte convection on the dissolution and loss of polysulfide. The sulfur loading is well known to have a great influence on the electrochemical performance of the sulfur/carbon composites (C/S). However, C/S should also leave a certain gap to prevent the volume expansion of active sulfur during  $\text{Li}^+$  insertion and promote the electrochemical reaction of the lithium sulfur battery [16]. For further retarding the polysulfide dissolution, reports about chemical interaction between polar nano-materials and polysulfides were becoming hotspots, such as metal oxide [17-20], MXenes [21] and conductivity polymers [22-25]. However, low utilization of sulfur was realized because of the poor electrical conductivity of metal oxides. Among the functionalized carbon materials, carbon materials doped with heteroatoms, such as N-doped graphene [26] and mesoporous carbon [27], B-doped reduced graphene oxide [28] are also investigated to retard the shuttle effect. These modified materials allow achieving better electrochemical performance than pristine carbon materials. However, the mentioned above processes are usually complicated and high cost, which leads to a lack of competitiveness of Li-S batteries.

To summary, the low electrochemical capacity of whole electrode in the charge-discharge process can be attributed to two reasons: (1) polysulfide ions are easily dissolved in the electrolyte; (2) the electrical conductivity of the carbon material is poor. Therefore, ideal carbon materials should satisfy with large free space for buffering volumetric expansion and connected conductive network. It is well known that, the conductivity of carbon materials always increases as the carbonization temperature increased because of the higher degree of graphitization. Carbon materials with high conductivity can effectively enhance the kinetic process, thus allow achieving high activity. In order to confirm this idea, in this work, we regulate the pore wall microstructures of the template mesoporous carbon materials (MC), and then use it as the conductive carrier to prepare the sulfur-carbon composites via the melt diffusion method. The electrochemical properties of the sulfur carbon composites are preliminarily investigated.

## 2. MATERIALS AND METHODS

### 2.1. Preparation of mesoporous carbon (MC-X)

Magnesium citrate (Tianjin Guangfu Fine Chemical Research institute, AR) was used as the

precursor of mesoporous carbon (MC) and provided nano-MgO templates. MC-1000 pyrolyzed at 1000 °C was obtained according to a similar procedure in our previous report [16]. Then, MC-1000 was heated to 1300, 1600, 2000, and 2800 °C for 1 h in nitrogen atmosphere, respectively. The MC materials will be described as MC-X, where 'X' represents the heat treatment temperature.

## 2.2 Preparation of mesoporous carbon/ sulfur (MC-X/S) composites

The mesoporous carbon /sulfur (MC/S) composites were prepared by melt diffusion method. MC-X was mixed with the high-purity sulfur (99.99%, Aladdin, AR) with weight ratio of 1:2, then ground into uniformity by ball-milling at 230 rpm. Finally, the MC/S composites were obtained after heating for 5 h at 150 °C in the muffle furnace and 3 h at 300 °C.

## 2.3. Materials characterization

Field-emission scanning electron microscopy (FE-SEM, Hitachi S-4800) and high-resolution transmission electron microscopy (HR-TEM, Tecnai G2 F20) were taken to observe the morphology and structure of MC-X and MC/S. SEM with energy-dispersive X-ray (EDX) spectroscopy was carried out via the FEI Nova Nano-SEM 450 at 10 kV. The N<sub>2</sub> adsorption-desorption isotherms were measured on Autosorb-iQ adsorption analyzer at 77K. The specific surface area, pore size distribution (PSD) and total pore volumes can be calculated by BET method and BJH model.

## 2.4 Electrochemical Measurement

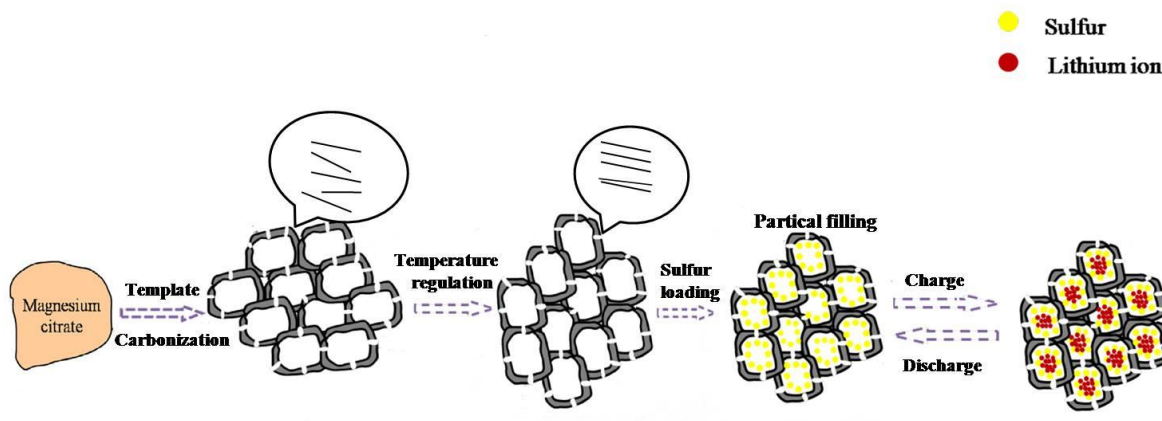
Active material (MC/S), conductive agent (carbon black) and binder (PTFE) with a weight ratio of 80:10:10 was mixed as slurry in NMP. By using a common doctor-blade coating method, the electrodes were obtained after drying for 12 h. And then CR2430 coin type cells were assembled as the way we had reported [16]. Land CT-2001A (Wuhan, China) used for GCD tests were performed at the voltage ranging from 1 V to 3 V. Cyclic voltammetry (CV) curves (CHI604D, China) were acquired at a scan rates of 0.1 mV/s.

# 3. RESULTS AND DISCUSSION

## 3.1. Characterizations of the MC-X and MC/S.

MC-X is fabricated via a simple high temperature carbonization process, and then modified by using a temperature-programmed route, as depicted in Scheme 1. Figure 1 and Table 1 presents the specific surface area and pore volume distribution of MC-X after modification. As seen in Figure 1, the specific surface area of MC-X was 1009, 1432, 1501, 1372, 920 and 168 m<sup>2</sup>g<sup>-1</sup>, respectively. The effect of temperature on the specific surface area is quite obvious, namely, as temperature increases up to

1300 °C, the specific surface area increases, then it decreases. When the temperature was 2800 °C, the specific surface area of MC-2800 sharply decreased to 168 m<sup>2</sup>g<sup>-1</sup>. Meanwhile, the pore volume of MC-X presented the same trend with the specific surface area and the max pore volume was 3.147 cm<sup>3</sup>g<sup>-1</sup>, which calculated by BET method (Table 1).



**Scheme 1.** Schematic diagram illustrating the preparation process of MC-X/S composite electrodes.

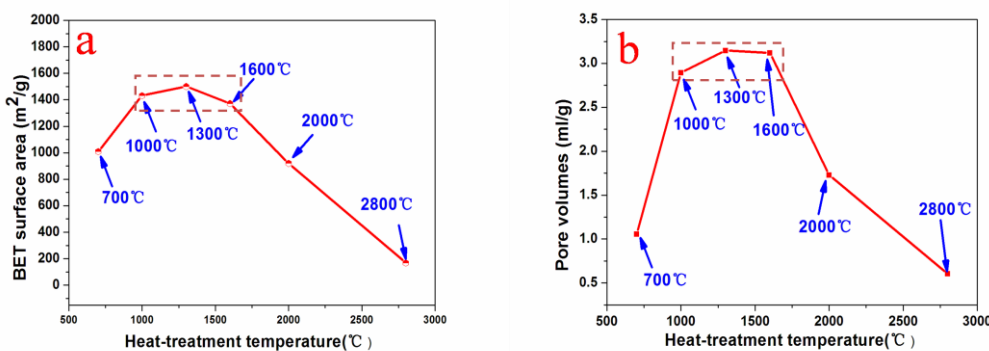


**Figure 1.** The specific surface area and pore volume of MC-X at different heating treatment temperature.

**Table 1.** The specific surface area and pore volume of MC-Xs treated at different temperature.

Samples	Temperature (°C)	Specific surface area (m <sup>2</sup> /g)	Pore volume (cm <sup>3</sup> /g)
MC-700	700	1009	1.056
MC-1000	1000	1432	2.894
MC-1300	1300	1501	3.147
MC-1600	1600	1372	3.120
MC-2000	2000	920	1.728
MC-2800	2800	168	0.605

In particular, the specific surface area and pore volume were not varied much when the temperature range was 1000 to 1600 °C, but sharply decreased at 2000 °C, this is because the graphite

micro-crystal structure gradually formed caused the pore wall structure changed dramatically. In order to study of the direct relation in between the micro-wall structure and the corresponding properties of MC-X, we chosen the same carbon source precursor, similar specific surface area and pore volume mesoporous carbon materials (1000, 1300 and 1600 °C) as the carbon matrix for MC/S composites.

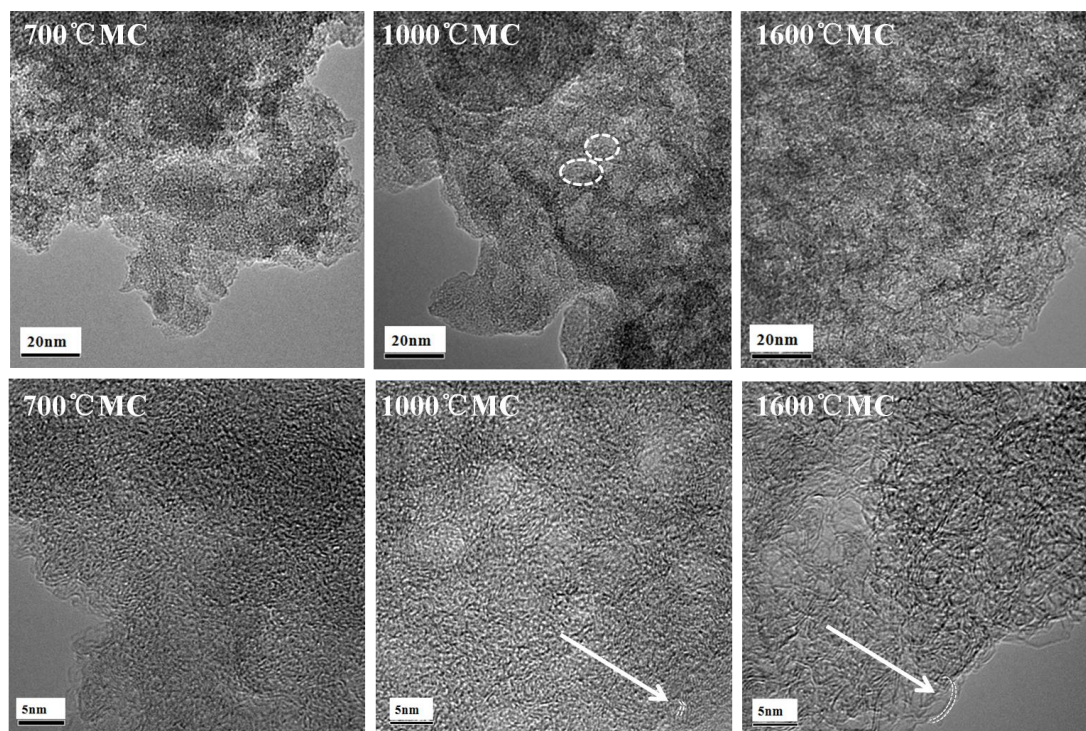


**Figure 2.** The HR-TEM images of MC-Xs.

The effect of temperature regulation on the microcrystalline structure of MC-X can be clearly observed by high rate transmission (HR-TEM). As shown in Figure 2, MC-1000 displays larger cluttered layers of 1~2 nm than that of MC-700, although the crystallites were still in a relatively short form (as shown in fig. 2b arrows). After modified at 1600 °C, the crystallites continued growth, and the six angle net structures layers gradually change into the graphited structure with regular orientation. The well alignment of graphited crystallites structure may enable the MC-X to have good electronic conductivity and further increase the activity of MC/S composites.

Nitrogen sorption isotherms was performed to characterize the variation of the specific surface area and pore volume of MC-X (1000, 1300,1600) before and after sulfur loading. The adsorption isotherms curves ascribed to three materials (Figure 3a, b, c black line) are classified into type IV which indicating abundant porous structure mainly consisting of meso- pores, according to IUPAC classification [29-31]. After sulfur loading, the volume of adsorbed nitrogen sharply reduced under the same relative pressure. When the relative pressure ( $P/P_0$ ) is 0~0.8, nitrogen was almost no longer adsorbed and a small amount of adsorption occurred until the relative pressure of  $P/P_0$  was close to 0.9. The pore size distribution curves before and after sulfur loading could also be seen in Fig. 3(d, e, f), which indicated a wealth of pore structure existing in the carbon matrix [29-31]. Table 2 clearly showed that the corresponding pore volume dramatically decreased after sulfur loading. Overall the

results indicate the elemental sulfur is successfully embedded in the mesopores of MC materials.

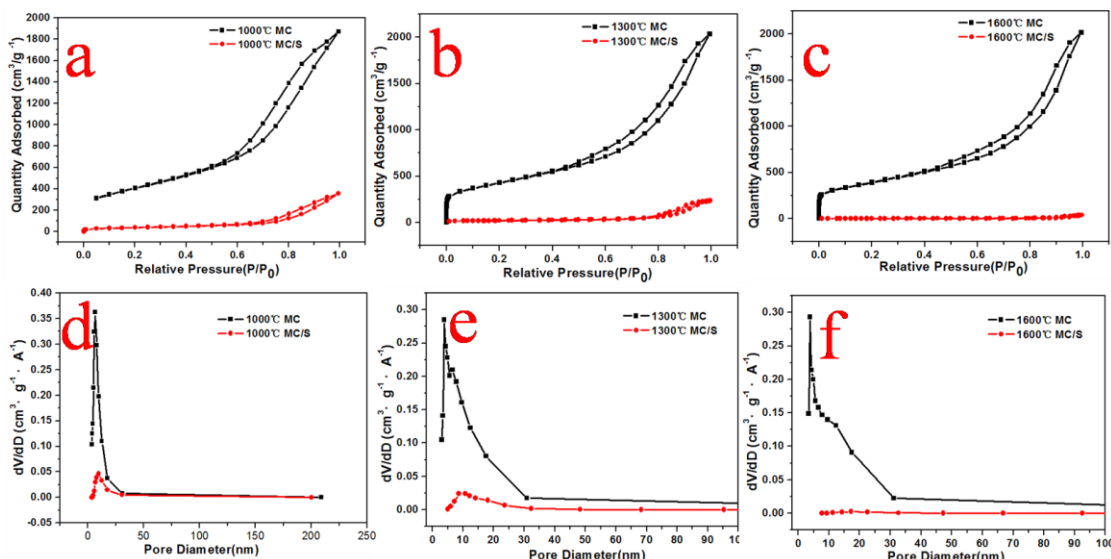


**Figure 3.** Nitrogen adsorption/desorption isotherms of MC-X before and after sulfur loading: a)1000°C,b)1300°C,c)1600°C; Pore size distribution curves of the MC-X before and after sulfur loading d)1000°C,(e)1300°C,(f)1600°C

**Table 2.** The specific surface area and pore volume of MC-Xs before and after sulfur loading.

Samples	Before sulfur loading		After sulfur loading	
	Specific surface area m <sup>2</sup> /g	pore volume cm <sup>3</sup> /g	Specific surface area m <sup>2</sup> /g	pore volume cm <sup>3</sup> /g
MC-1000	1432	2.894	133	0.353
MC-1300	1501	3.147	75	0.370
MC-1600	1372	3.120	8	0.060

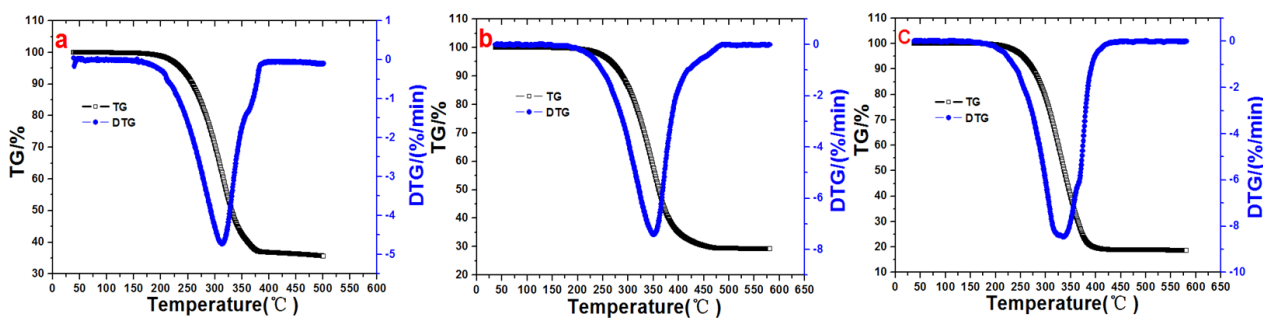


**Figure 4.** TGA curves of MC-X/S composites :a)1000°C MC/S, b)1300°C MC/S and c) 1600°C MC/S.

TGA (Fig. 4) analyses were performed to confirm the accurate content of sulfur in the MC-X/S composite cathode. According to the MC/S ratio of 1:2, we can calculate the theoretical adding amount

of sulfur was 66.7 %. When the temperature is 300~350°C, the weight loss is the fastest which corresponding to the sulfur loss. In accordance with the weight loss of sulfur, the actual sulfur loading was 63, 67 and 76 %, which were almost consistent with the theoretical value.

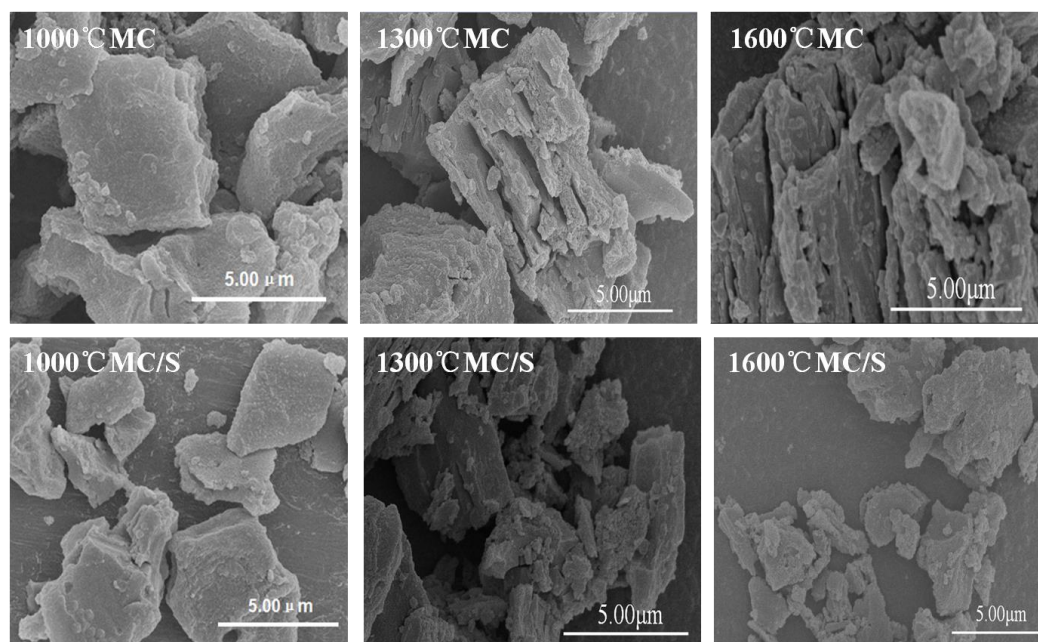


Figure 5. The SEM images of MC-Xs and MC-X/S.

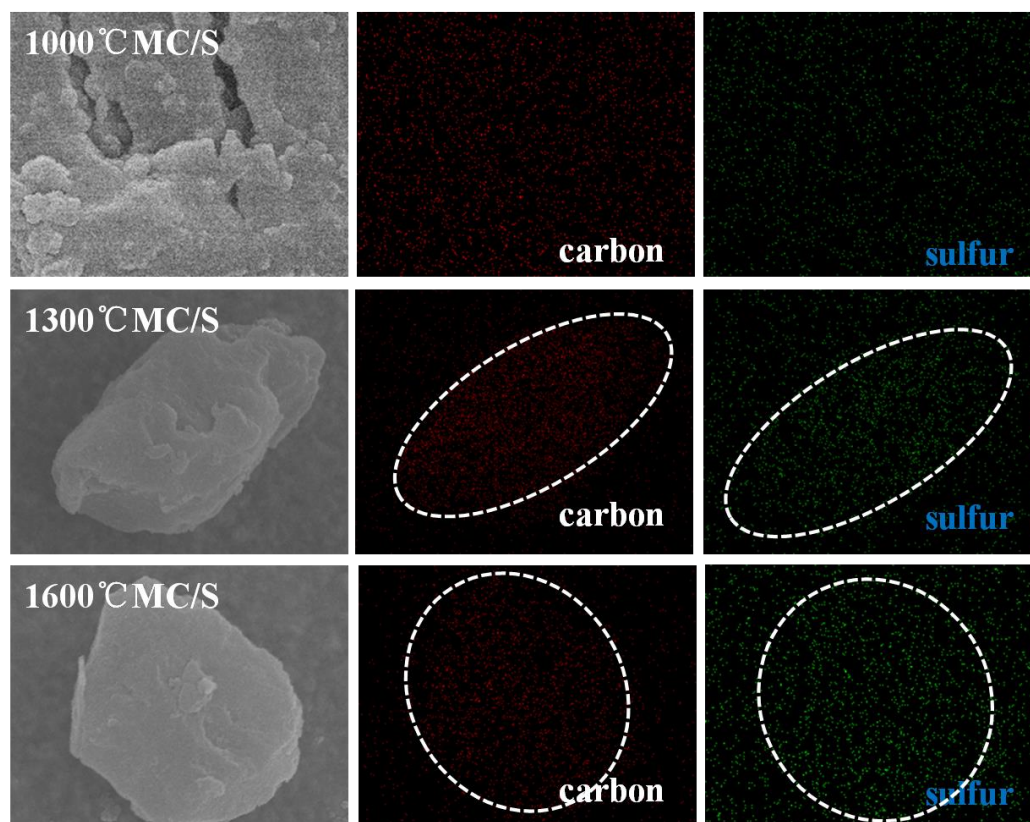
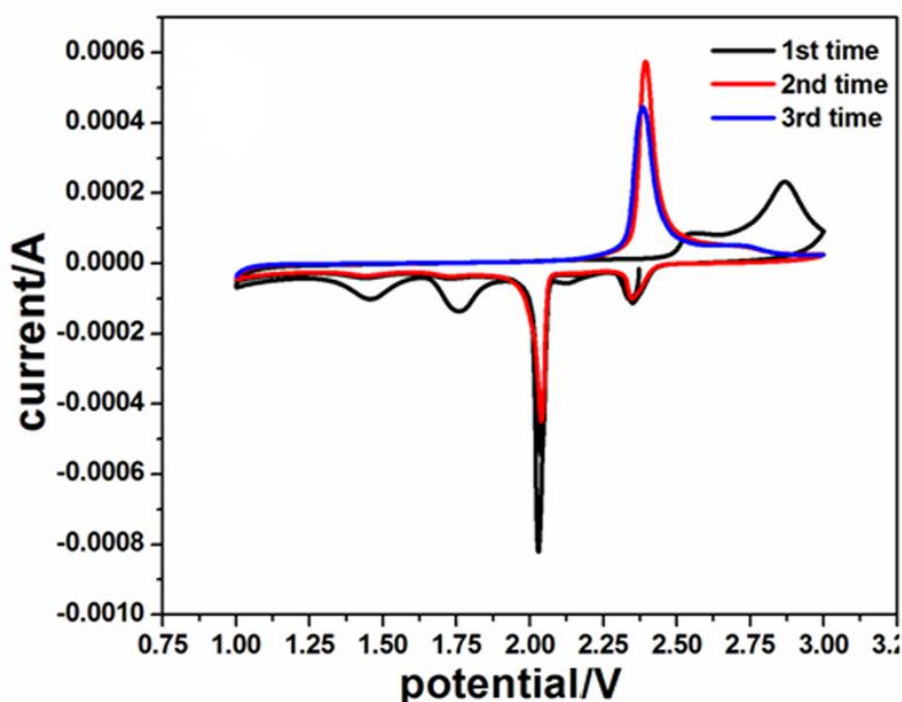


Figure 6. SEM-EDX images of MC-X/S.

Figure 5 shows the SEM images of MC-X (1000, 1300, 1600) before and after sulfur loading. The upside is the raw material images and the below was the images of MC/S composites. It could be seen that the size of the MC-X particles changes slightly before and after sulfur loading indicating that the sulfur has successfully entered into the nanopores of MC-X and no deposition on the surface of MC-X. To investigate the distribution of sulfur in the MC/S, the SEM-EDX spectra of MC/S with different micro wall structure were taken. From figure 6, the carbon and sulfur mapping of MC-X/S clearly illustrated that sulfur nanoparticles were indeed homogeneously dispersed in the MC-X matrix within the mesopore [16]. The high loading and good dispersibility of sulfur may allow to better electrochemical characteristic of Li/S battery.

### 3.2. Electrochemical performance



**Figure 7.** CV curves of the MC-1000/S at scan rate of  $0.1 \text{ mV s}^{-1}$

Taking MC-1000/S for example, cyclic voltammetry (CV) was performed between 3.0 and 1.0 V at the scan rate of  $0.1 \text{ mV s}^{-1}$ . The curves present the typical sulfur cathode CV behavior in Figure 7 [32]. Three cathodic peaks identified in the spectra are corresponding to the typical reduction of elemental sulfur ( $\text{S}_8$ ) to  $\text{S}_6^{2-}$ ,  $\text{S}_4^{2-}$ , and  $\text{S}_2^{2-}$  (or  $\text{S}_2$ ), respectively. Actually, the reactions occurred during the charge/discharge process was too complicated that the reduction and oxidation peak areas are not one-to-one, which was different from the conventional battery system. As the progress continued, reduction and oxidation peaks both shifted, but reduction peak increased and oxidation potential shifted to lower potential. The phenomena displayed that  $\text{Li}_2\text{S}_n$  complexes with lower adsorption energy formed after the first anodic oxidation [33]. These may be in favor of the improvement of cycle

life of the electrode.

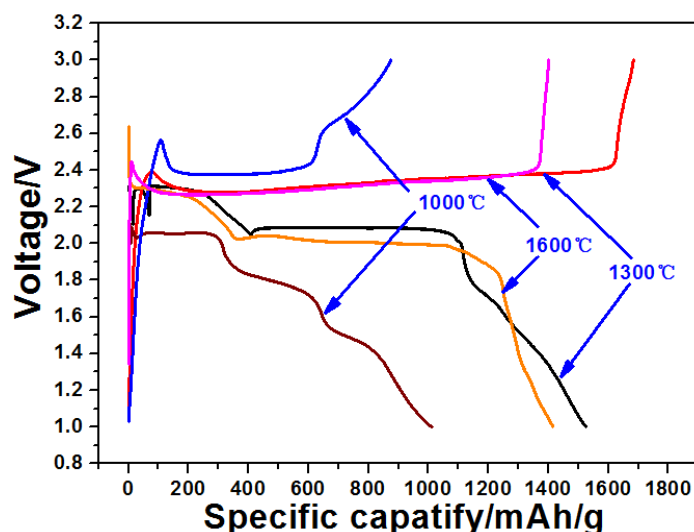


**Figure 8.** First charge/discharge curves of the MC-X/S composite cathodes at a current density of 200 mA g<sup>-1</sup>

**Table 3.** Comparison of the MC-X cathode in this work with reported results

Cathode materials	Discharge capacity (mAh/g)	Sulfur loading (%)	Ref.
Sulfur/graphene/carbon <sup>a</sup> nanotubes composites <sup>a</sup>	1468	57	12
Graphene@microporous carbon <sup>a</sup>	1320	60	9
Flexible nanostructure paper <sup>a</sup>	1234	56	14
3D graphene/sulfur <sup>a</sup>	1077	90	15
PVP/ GA <sup>a</sup>	1192	63	25
MC-1300 <sup>b</sup>	1524	67	(this work)

**Note:** Working Conditions: a) 0.1 C; b) 200 mAh/g

First discharge voltage profiles of Li/S battery based on MC-1000/S appeared three discharge reaction plateaus, which was coincided with the CV results. As shown in Figure 8, S<sub>8</sub> was reduced to highly oxidized polysulfides Li<sub>2</sub>S<sub>8</sub> and Li<sub>2</sub>S<sub>6</sub> at 2.10 V (vs. Li<sup>+</sup>/Li) in the upper plateau, the plateau at 1.75 V (vs. Li<sup>+</sup>/Li) corresponding to the reduction of Li<sub>2</sub>S<sub>8</sub> and Li<sub>2</sub>S<sub>6</sub> to Li<sub>2</sub>S<sub>4</sub>, and Li<sub>2</sub>S<sub>4</sub> or lower sulfides was finally reduced to Li<sub>2</sub>S<sub>2</sub> or Li<sub>2</sub>S at 1.40 V. However, for MC-1300/S and MC-1600/S, there were two obvious voltage platforms at 2.1 V and 2.3 V, which corresponded to the transformation of S<sub>8</sub> molecules to high oxidized polysulfide ions S<sub>x</sub><sup>2-</sup> (x=4~6), as well as the further reduction of S<sub>x</sub><sup>2-</sup> to the final reduction Li<sub>2</sub>S<sub>2</sub> and Li<sub>2</sub>S [34-36]. The charging voltage platform of 2.3~2.4 V was stable in the subsequent charging process. According to the data in Figure 8, the discharge capacity of MC-1000/S, MC-1300/S and MC-1600/S were 1083, 1524 and 1415 mAhg<sup>-1</sup>, respectively. Compare to

MC-1000/S, the first charge discharge capacity of MC-1300/S and MC-1600/S was much higher which may attribute to the relatively higher conductivity of MC-X by high temperature modification. In addition, the resulting capacity of MC-X/S samples is clearly higher than the most of previously reported materials which are listed in Table 3. The high temperature modification may yield to high conductivity, which is conducive to the activity and utilization of elemental sulfur.

At the current density of 200 mAh g<sup>-1</sup>, cycling performance of the MC-X/S with different micro-wall structure was shown in Figure 9. It can be seen that the initial discharge capacity of the batteries of MC-1300/S and MC-1600/S is higher than that of MC-1000/S, but the deceleration rate of MC-1300/S is slower than that of other batteries. Especially, MC-1300/S had shown the highest discharge capacity of 1524 mAh g<sup>-1</sup> which was closed to the theoretical specific capacity (1675 mAh g<sup>-1</sup>), and its corresponding specific surface area and pore volume was also the highest. Compared to micro structure, the sulfur loading percent seemed to have a minimal impact on the electrochemical performance. Nazar's group confirmed that 75% was the critical value of sulfur loading, specific capacity had little change when sulfur loading in excess of 75% but increased linearly with the sulfur loading within 75% [37]. Therefore, although the sulfur loading of MC-1600/S was higher than that of MC-1300/S, the performance of MC-1300/S was much better. The results demonstrated that pore structure played an important role in the inhibition of the dissolution of intermediate products. Moreover, the high conductivity of the carbon matrix improves the activity of the sulfur electrode, which is conducive to the electrochemical reaction of the whole electrode.

#### 4. CONCLUSIONS

In this work, template method is used to prepare mesoporous carbon materials (MC), and the pore wall microstructures are regulated via a temperature-programmed route. Then, MC materials with similar surface area and large pore volume are selected for further research. The influence of MC matrix microstructure on the electrochemical behavior of elemental sulfur is studied. The main results are as follows: for one part, MC with high specific surface, large pore volume and open phase channel structure provides a sufficient reaction place for the active substances, which has a great influence on the inhibition of disulfide dissolution and loss; for another part, the regulation of the microwall structure of MC increases the degree of graphitization of the MC-X, promoting the electronic conductivity of MC. Therefore, MC-1300 and MC-1600 present the high capacity of 1524 mAhg<sup>-1</sup> and 1415 mAhg<sup>-1</sup>, respectively, which is close to the theoretical specific capacity. The as shown microstructures regulated progress of MC can be used in any field where mesoporous structures are adopted.

#### ACKNOWLEDGEMENTS

This research was financially supported by the National Nature Science Foundation of China (51603147).

## References

1. P.G. Bruce, S.A. Freunberger, L.J. Hardwick and J.M. Tarascon, *Nat. Mater.*, 11 (2012) 19.
2. A. Manthiram, Y. Fu, S.H. Chung, C. Zu and Y.S. Su, *Chem. Rev.*, 114 (2014) , 11751–11787.
3. A. Manthiram, S.H. Chung, C. Zu, *Adv. Mater.*, 27 (2015) 1980.
4. J.M. Tarascon, M. Armand, *Nature*, 414 (2001) 359.
5. L.F. Nazar, M. Cuisinier and Q. Pang, *M R S Buletin*, 39 (2014) 436.
6. S. Chen, X. Huang, B. Sun, J. Zhang, H. Liu and G. Wang, *J. Mater. Chem. A.*, 2 (2014), 16199.
7. Y. Yang, G. Zheng and Y. Cui, *Chem. Soc. Rev.*, 42 (2013), 3018.
8. N. Jayaprakash, J. Shen, S.S. Moganty, A. Corona and L.A. Archer, *Angew. Chem. Int. Ed.*, 123 (2011), 6026.
9. N.W. Li, Y.X. Yin and Y.G. Guo, *RSC Adv.*, 6 (2016) 617.
10. M.D. Walle, Z. Zhang, X. You, M. Zhang, J.M. Chabu, Y. Li and Y.N. Liu, *RSC Adv.*, 6 (2016) 78994.
11. Y.L. Ding, P. Kopold, K. Hahn, P.A. van Aken, J. Maier and Y. Yu, *Adv. Funct. Mater.*, 26 (2016) 1112.
12. G. Yuan, G. Wang, H. Wang and J. Bai, *J. Nanoparticle Res.*, 17 (2015) 36.
13. J. Guo, Y. Xu and C. Wang, *Nano Lett.*, 11 (2011) 4288.
14. J. Cao, C. Chen, Q. Zhao, N. Zhang, Q. Lu, X. Wang, Z. Niu and J. Chen, *Adv. Mater.*, 28 (2016) 9629
15. B. Papandrea, X. Xu, Y. Xu, C.Y. Chen, Z. Lin, G. Wang, Y. Luo, M. Liu, Y. Huang, L. Mai, *Nano Res.*, 9 (2016) 240.
16. J. Wang, Y.H. Wu, Z.Q. Shi, C.C. Wu, *Electrochim. Acta*, 144 (2014) 307.
17. J. Zhang, Y. Shi, Y. Ding, W. Zhang, G. Yu, *Nano Lett.*, 16 (2016) 7276.
18. J.Y. Hwang, H.M. Kim, S.K. Lee, J.H. Lee, A. Abouimrane, M.A. Khaleel, I. Belharouak, A. Manthiram, Y.K. Sun, *Adv. Energy Mater.*, 6 (2016) 12886.
19. X. Wang, G. Li, J. Li, Y. Zhang, A. Wook, A. Yu, Z. Chen, *Energy Environ. Sci.*, 9 (2016) 2533.
20. Y. Tao, Y. Wei, Y. Liu, J. Wang, W. Qiao, L. Ling, D. Long, *Energy Environ. Sci.* 2016, 9, 3230.
21. X. Liang, Y. Rangom, C.Y. Kwok, Q. Pang, L.F. Nazar, *Adv. Mater.*, 29 (2017) 1603040.
22. L.F. Xiao, Y.L. Cao, J. Xiao, B. Schwenzer, M.H. Engelhard, L.V. Saraf, Z.M. Nie, G.J. Exarhos, J. Liu, *Adv. Mater.*, 24 (2012) 1176.
23. Y. Yang, G.H. Yu, J.J. Cha, H. Wu, M. Vosgueritchian, Y. Yao, Z.N. Bao, Y. Cui, *ACS Nano.*, 5 (2011) 9187.
24. Y.F. Dong, S.H. Liu, Z.Y. Wang, Y. Liu, Z.B. Zhao, J.S. Qiu, *Nanoscale*, 7 (2015) 7569.
25. B.Y. Li, Q. Xiao, Y.Z. Luo, *RSC Adv.*, 7 (2017) 54453.
26. J. He, K. Zhou, Y. Chen, C. Xu, J. Lin and W. Zhang, *Mater. Today Energy*, 1-2 (2016) 11.
27. Y.J. Hao, Z.Q. Shi, J. Wang and Q. Xu, *RSC Adv.*, 5 (2015) 31629.
28. Y. Tian, C.L. Deng, Z.H. Sun, Y. Zhao, T.Z. Tan, F.X. Yin, X. Wang, *Int. J. Electrochem. Sci.*, 13 (2018) 3441.
29. S. Du, L. Wang, X. Fu, M. Chen, C. Wang, *Bioresour. Technol.*, 139 (2013) 406-409.
30. K. Xi, S. Cao, X.Y. Peng, C. Ducati, R.V. Kumar, A.K. Cheetham, *Chem. Commun.*, 49 (2013) 2192.
31. G.Y. Xu, B. Ding, L.F. Shen, P. Nie, J.P. Han, X.G. Zhang, *J. Mater. Chem. A.*, 1 (2013) 4490.
32. H. Yamin, A. Gorenshstein, J. Penciner, Y. Sternberg, E. Peled, *J. Electrochem. Soc.*, 135 (1988) 1045.
33. H. Wang, Y. Yang, Y. Liang, J.T. Robinson, Y. Li, A. Jackson, Y. Cui, H. Dai, *Nano Lett.*, 11 (2011) 2644.
34. Y.J. Choi, Y.D. Chung, C.Y. Baek, K.W. Kim, H.J. Ahn, *J. Power Sources*, 184 (2008) 548.
35. C. Lai, X.P. Gao, B. Zhang, T.Y. Yan, Z.J. Zhou, *Phys. Chem. C*, 113 (2009) 4712.
36. H. Yamin, E. Peled, *J. Power Sources*, 9 (1983) 281.

37. J. Schuster, G. He, B. Mandlmeier, T. Yim, K.T. Lee, T. Bein, L.F. Nazar, *Angew. Chem. Int. Ed.*, 50 (2011) 5904.

© 2018 The Authors. Published by ESG ([www.electrochemsci.org](http://www.electrochemsci.org)). This article is an open access article distributed under the terms and conditions of the Creative Commons Attribution license (<http://creativecommons.org/licenses/by/4.0/>).